Noname manuscript No.
(will be inserted by the editor)

Water Transport Through (7,7) Carbon Nanotubes of Different Lengths using Molecular Dynamics

William D. Nicholls · Matthew K. Borg · Duncan A. Lockerby · Jason M. Reese

Received: date / Accepted: date

Abstract Non-equilibrium molecular dynamics simulations are used to investigate water transport through (7,7) CNTs, examining how changing the CNT length affects the internal flow dynamics. Pressure-driven water flow through CNT lengths ranging from 2.5 nm to 50 nm is simulated. We show that under the same applied pressure difference an increase in CNT length has a negligible effect on the resulting mass flow rate and fluid flow velocity. Flow enhancements over hydrodynamic expectations are directly proportional to the CNT length. Axial profiles of fluid properties demonstrate that entrance and exit effects are significant in the transport of water along CNTs. Large viscous losses in these entrance/exit regions lead into central "developed" regions in longer CNTs where the flow is effectively frictionless.

Keywords Molecular dynamics · Carbon nanotubes · Water flow

1 Introduction

Recent experiments [1–3] and molecular dynamics (MD) simulations [4–7] have shown that water is transported through carbon nanotubes (CNTs) at unexpectedly high flow rates. The contained fluid structure has also been shown to be dependent upon the CNT diameter: single-file molecule chains at the smallest diameters and bulk-like structures at larger diameters. The flow of water inside CNTs of diameters below 1.66 nm can be regarded as non-continuum: the problem cannot be accurately described using conventional continuum fluid mechanics with its associated linear constitutive relations and no-slip boundary conditions [8]. This truly atomistic problem requires a molecular dynamics simulation method.

To investigate the transport of water through CNT membranes it is necessary to consider each CNT independently, because both the fluid structuring and mass flow rate vary with its diameter. Mass flow rate decreases with decreasing CNT diameter, before increasing when approaching the smallest diameters penetrable by water [4]. It is clear that no single hydrodynamic theory can be applied to fluid flow through all CNTs, and the choice of CNT is dependent upon the application of interest.

CNTs aligned within a membrane [9] present new opportunities for selective material separation, including sea water desalination. Recent MD simulations have indicated that the (7,7) CNT, which has a diameter of 0.96 nm, may possess the optimum attributes for desalination, removing 95% of salt while transporting water at a suitably high flow rate [5, 10]. CNTs with smaller diameters than the (7,7) have a lower flow rate, while larger diameter CNTs do not remove enough salt from the water for human consumption. Previous studies have shown that there is no correlation between the CNT chirality and the internal fluid structure at diameters below 1.39 nm [4]. So CNTs with different chiralities but the same diameter should produce similar results. For these reasons in this paper we choose to investigate pressure-driven water flow through (7,7) CNTs.

W.D. Nicholls · M.K. Borg · J.M. Reese
Department of Mechanical & Aerospace Engineering, University of Strathclyde, Glasgow G1 1XJ, UK
Tel.: +44-141-5484386
E-mail: william.nicholls@strath.ac.uk

D.A. Lockerby
School of Engineering, University of Warwick, Coventry CV4 7AL, UK

Another important characteristic of CNTs is their length. CNT membranes as thin as 2-5 μm can be manufactured [9, 11] but MD simulations are typically performed using CNTs which are only a few nanometers in length. Previous simulations investigating the effect of CNT length were performed using short CNTs where changes in length were by a few nanometers. Mattia and Gogotsi [12] suggest that the length of the carbon nanotube is the primary determiner of the nature of the flow: in very short CNTs stochastic flow, due to thermal fluctuations, has been observed [13]; in infinitely long CNTs, modelled using periodic boundary conditions, single file diffusion dominates [14], as also seen experimentally. Understanding the influence of length on the flow is of central importance to understanding the nature of CNT flows in general. In this paper, we use MD simulations to investigate water transport along (7,7) CNTs with lengths ranging from 2.5 to 50 nm, and examine how the length affects fluid flow velocity, mass flow rate and axial fluid properties.

2 Simulation Methodology

Our simulations are performed using *mdFoam* [15–18], a new parallelised non-equilibrium molecular dynamics solver, that is open-source and available to download from [19]. The motion of molecules in an MD simulation is governed by Newton's second law, and the equations of motion are integrated using the Verlet leapfrog scheme. A time-step of 1 fs is used in all the following simulations.

The rigid TIP4P water model is used, which consists of a Lennard-Jones (LJ) interaction potential at the oxygen atom site (O), positive Coulomb charges at the two hydrogen sites (H) and a negative charge at a site M, located above O along the bisector of the HOH angle. The O-O LJ interactions use the following parameters: $\sigma_{OO} = 3.154$ Å and $\epsilon_{OO} = 0.6502$ kJ mol^{-1}. The electrostatic point charge values for water are -0.8476e and +0.4238e for the M and hydrogen sites, respectively. The carbon-water interaction is solely represented by a carbon-oxygen LJ potential using the following parameters: $\sigma_{CO} = 3.19$ Å and $\epsilon_{CO} = 0.392$ kJ mol^{-1} [20]. Electrostatic and LJ interactions are smoothly truncated at 1.0 nm.

The configuration of our pressure-driven flow simulation domain is shown in Fig. 1. Two graphene sheets are positioned at the inlet and outlet of the CNT to form a simplified membrane representation. The CNT and graphene sheets are modelled as rigid structures to speed up the MD runs: this has been reported to be a fair approximation in a previous study [6]. Periodic boundary conditions are employed in the y- and z-directions, while non-periodic boundary conditions are applied in the x-direction: the left-hand boundary is a specular-reflective wall, while the right-hand boundary deletes molecules upon collision. The wall helps control the fluid pressure and density upstream while the deletion patch creates an open system [21]. A pressure difference of 200 MPa is applied across the membrane in all simulations; such a large pressure difference is required to resolve the dynamics of the simulation over a shorter time period due to the large computational cost associated with MD. (Pressure differences of 5-7 MPa are generally used in industrial filtration processes, but the resulting flows rates are too low for MD to accurately resolve over a practical timescale.) Berendsen thermostats are applied to both fluid reservoirs to maintain a constant temperature of 298 K and eliminate the contribution of any temperature gradients to the fluid transport. The fluid is not controlled inside the CNT so as not to disturb the dynamics of the contained water molecules. The maximum variation in water temperature inside any CNT we found to be 3.5 K. Both fluid reservoirs have dimensions of 4.4×4.4×4.4 nm^3. The number of molecules in the entire domain ranged from ∼7000 to ∼13000 for the shortest to the longest CNTs, respectively.

The upstream pressure is controlled using a proportional-integral-derivative (PID) control feedback loop algorithm, similar to that used in [18], in addition to adaptive control of mass-flux at the inlet. An external force is distributed over all molecules which reside in control zone 1 to create the required pressure in the neighbouring sampling region, see Fig. 1. The required external force is calculated using three separate components: a proportional term, an integral term, and a derivative term. The proportional force term is calculated from the pressure error $e_p = p^t - \langle p \rangle$ between the measured pressure in the sampling region $\langle p \rangle$ and the target pressure p^t:

$$\mathbf{f_p} = K_p \frac{e_p A \hat{\mathbf{n}}}{N}, \tag{1}$$

where A is the cross-sectional area of the control zone, $\hat{\mathbf{n}}$ is a normal vector indicating the direction of the applied force, K_p is the proportional gain (dimensionless), and N is the number of molecules in the control region. The integral force term is calculated using the accumulation of past pressure errors:

$$\mathbf{f_i} = K_i \frac{\left(e_p^n + e_p^o\right) \Delta t_m A \hat{\mathbf{n}}}{2N}, \tag{2}$$

where e_p^n is the pressure error at the new time step n, e_p^o is the accumulated pressure error at the old time step o, Δt_m is the MD time step size, and K_i is the

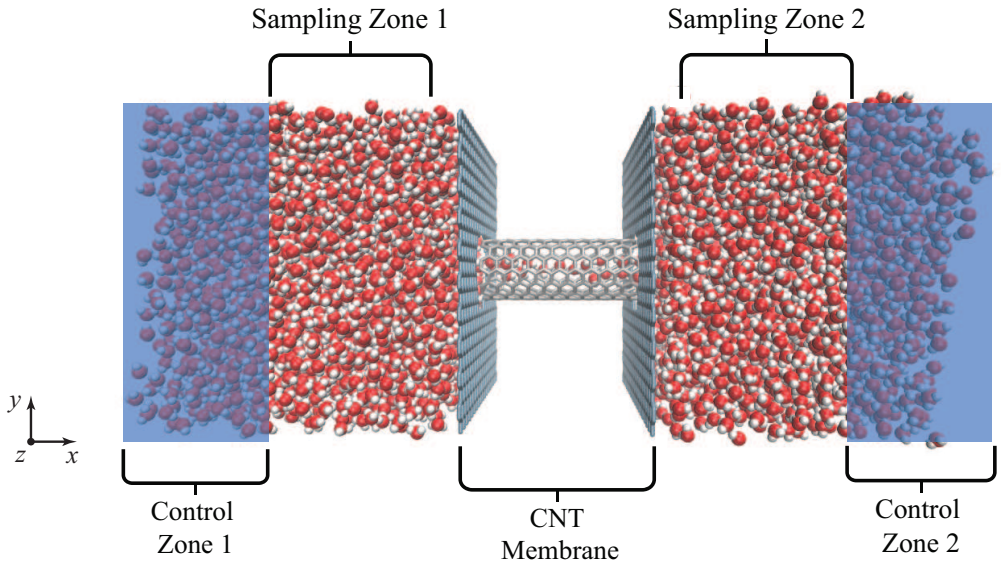

Fig. 1: Simulation domain.

integral gain (units are s^{-1}). The derivative force term is calculated using the rate of change of the pressure error:

$$\mathbf{f_d} = K_d \frac{\left(e_p^n - e_p^o\right) A\hat{\mathbf{n}}}{\Delta t_m N}, \tag{3}$$

where K_d is the derivative gain (units are s). The equation of motion for a molecule, j located in control zone 1 is then:

$$\mathbf{a_j} = \mathbf{f_j}/m_j + \mathbf{f_t^{ext}}/m_j, \tag{4}$$

where $\mathbf{a_j}$ is the acceleration of molecule J, m_j is the molecule mass, $\mathbf{f_j}$ is the total intermolecular force, and $\mathbf{f_t^{ext}}$ is the total external force given by the sum of all three PID components:

$$\mathbf{f_t^{ext}} = \mathbf{f_p} + \mathbf{f_i} + \mathbf{f_d}. \tag{5}$$

A mass flux of water molecules is imposed at the inlet of the system in order to compensate for those molecules that leave the system, and to keep the upstream reservoir in a steady thermodynamic state. Our numerical implementation controls density adaptively in the inlet control zone: the target mass density in the control zone is set to the measured fluid density in the sampling region, because the pressure and temperature of the fluid in this region are set at the desired values. The pressure control process helps in establishing a steady and homogeneous density distribution because it forces molecules in or out of control zone 1. We use relaxation to improve the stability of our algorithm, so the target density within the control zone is given by:

$$\rho^t = \beta\langle\rho_s\rangle + (1-\beta)\langle\rho_c\rangle, \tag{6}$$

where $\langle\rho_s\rangle$ is the measured density in sampling zone 1, $\langle\rho_c\rangle$ is the measured density in control zone 1, and β is a relaxation parameter (e.g. ∼0.5). The number of molecules to insert/delete in control zone 1 is then:

$$\Delta N = \frac{(\rho^t - \langle\rho_c\rangle)V_c}{m}, \tag{7}$$

where V_c is the volume of the control zone and m is the mass of a water molecule. For molecule insertions, the USHER algorithm [22] is used, which searches for a site within the potential energy landscape via a steepest-descent iteration scheme.

Downstream of the membrane, pressure is controlled using a pressure-flux technique [23] in order to allow the flow through the system to develop without being over-constrained. The pressure in sampling zone 2 is set by applying an external force to all molecules in control zone 2:

$$\mathbf{f^{ext}} = \frac{p^t A\hat{\mathbf{n}}}{N}, \tag{8}$$

where p^t is the target pressure. A key advantage of these pressure control techniques is that the required reservoir pressures can be applied explicitly.

Five different CNT lengths are investigated: 2.5, 5.0, 12.5, 25, and 50 nm. Initially the CNT is closed while the reservoirs are filled with water molecules and equilibrated to the correct conditions. After this initial equilibration, the CNT is opened and allowed to fill naturally. Once the number of molecules in each CNT has reached a constant value the simulation is allowed to proceed until the flow rate reaches a steady state value. Each

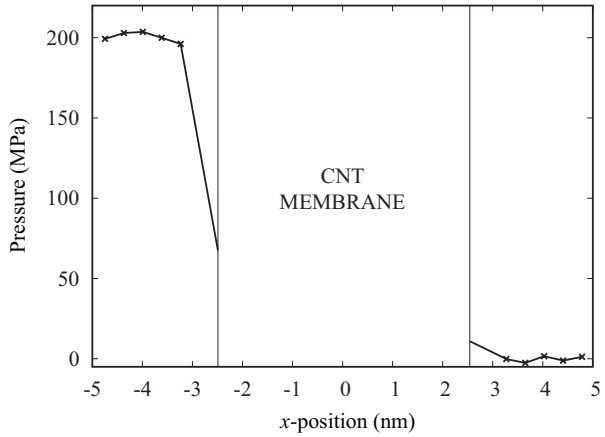

Fig. 2: MD results of pressure profile across domain showing the application of a 200 MPa pressure difference.

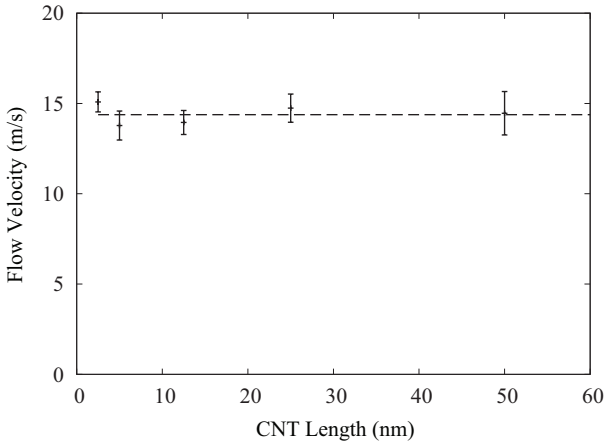

Fig. 3: Relationship between flow velocity and CNT length under a 200 MPa pressure difference. The horizontal dashed line indicates an average fluid velocity of 14.6 m/s.

simulation is then advanced by a further 2 ns before averaging of properties is performed. All data presented in this paper is from a 4 ns averaging period.

The same pressure difference of 200 MPa is imposed across all the CNT membranes, see Fig 2, and the downstream reservoir is maintained at atmospheric conditions. Pressure is calculated from the stress tensor using the Irving-Kirkwood method. The maximum variation in the applied pressure difference between any of the simulation runs was measured to be 0.8 MPa. The uncertainty in the pressure difference is calculated from the variation in the mean pressure difference between the two reservoirs.

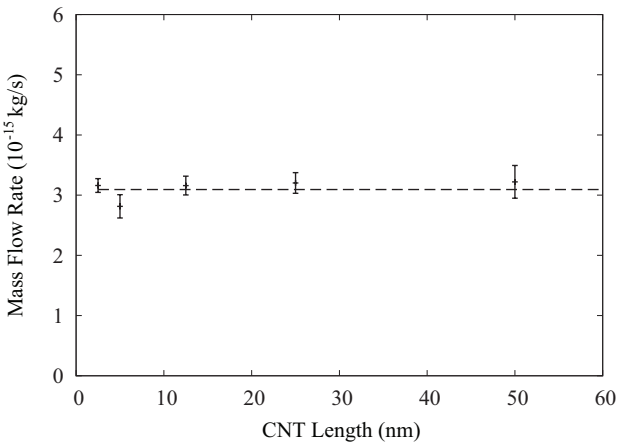

Fig. 4: Relationship between mass flow rate and CNT length under a 200 MPa pressure difference. The horizontal dashed line indicates an average mass flow rate of 3.11×10^{-15} kg/s.

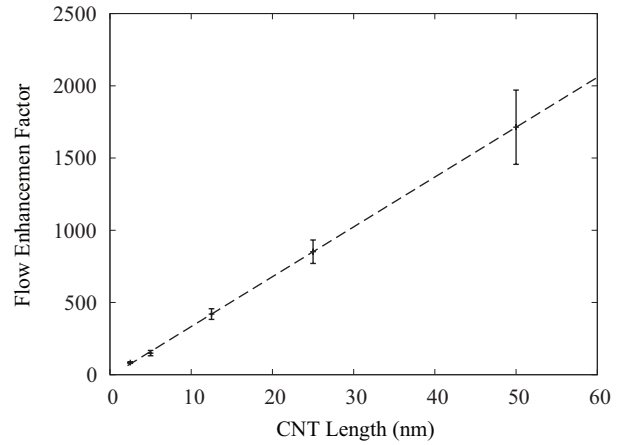

Fig. 5: Flow enhancement factors (over hydrodynamic predictions) for different CNT lengths.

3 Results and Discussion

3.1 Flow Velocity and Mass Flow Rate

The average fluid streaming velocity for the different nanotube lengths under the same applied pressure difference are shown in Fig. 3. The fluid velocities are measured within the same 1 nm long region located at the midpoint of each CNT. We find that there is no significant change in the fluid streaming velocity as the CNT length increases from 2.5 nm to 50 nm. In this range of lengths, the average fluid velocity is measured to be 14.6 m/s. Previous studies have found that small changes in nanotube length (a few nanometers longer) had no effect on the fluid flow rate under the same pressure difference [5]. We can confirm that this phenomenon holds for extensions of 20 times the original length.

It has also previously been shown that there is a linear relationship between the applied pressure difference and the resulting fluid mass flow rate and fluid velocity [5,7]. By using this relationship we are able to compare our average fluid velocity with that of Thomas and McGaughey [8]. They predicted a flow velocity of 5.2 m/s under a pressure difference of 73.5 MPa for a (7,7) CNT; extrapolating these values would predict a value of 14.2 m/s for a pressure difference of 200 MPa which is in good agreement with the flow velocities presented here.

The result in Fig. 3 is seemingly in contradiction to the results of Thomas and McGaughey (Fig. 3 in [8]), who demonstrate an increase of flow velocity with applied pressure gradient; in our results the applied pressure gradient ($\Delta P/L$) is also varied, but there is no significant change in flow velocity. The contradiction only arises, though, if one assumes that the pressure gradient alone is sufficient to characterise the driving force of the flow (which is the case in classical fluid mechanics). In fact, our results suggest that, because the nanotube flow velocity is relatively independent of L, it is perhaps the pressure drop, ΔP, which is the characteristic flow driver and not the pressure gradient. If this is the case, the contradiction is resolved: in the simulations of Thomas and McGaughey it is the increased pressure difference (ΔP) that is responsible for the increase in velocity they observed, and not the fact that the pressure gradient was changing; in our simulations, with ΔP fixed, the flow velocity is relatively unaffected.

A similar constant relationship is present between the mass flow rate and CNT length, shown in Fig. 4. As the fluid flow is non-continuum, the net flow rate is measured by averaging the number of molecules which cross a perpendicular plane located at the midpoint of each CNT over a prescribed time period; molecules which cross in the positive x-direction are counted as positive to the flow rate and those which cross in the opposite direction are counted as negative. The average mass flow rate through each CNT we calculated to be 3.11×10^{-15} kg/s. The measured flow rates can be compared to equivalent hydrodynamic flow rates via the no-slip Hagen-Poiseuille relation for flow in a cylindrical pipe:

$$\dot{m} = \frac{\pi r^4 \rho \Delta P}{8\mu L}, \tag{9}$$

where r is the radius of the CNT, ΔP is the pressure difference, ρ is the fluid density, μ is the dynamic viscosity, and L is the CNT length. The radius used here is related to the volume which the water can occupy inside a CNT. We take the radius within which 95% of the fluid resides, which was found to be 0.186 nm.

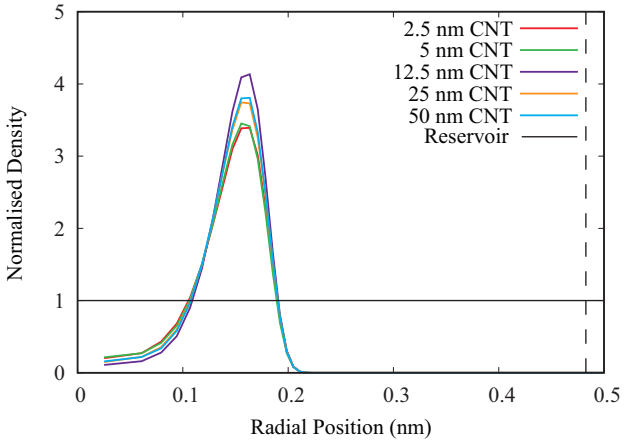

Fig. 6: Radial density distributions normalised with the reservoir density for CNTs of different lengths. Measurements are taken at the midpoint of each CNT length. The vertical dashed line indicates the position of the CNT surface.

Bulk properties for ρ and μ for water at 298 K are used. While this equation is not strictly valid in this flow problem, we wish to make a comparison with hydrodynamic predictions.

The flow enhancement factor, i.e. the ratio of our measured mass flow rate to the hydrodynamic prediction, shows a linear relationship with CNT length, see Fig. 5. In contrast to what is predicted by hydrodynamic theory, at these large pressure differences the mass flow rate does not decrease with increasing pipe length but remains constant over the lengths considered in this study. Flow enhancement values are in agreement with those reported by Corry [5] of $\mathcal{O}(10)$ at the shortest lengths, and Thomas and McGaughey [8] of $\mathcal{O}(1000)$ at the longest lengths. The reduction of the flow enhancement factor is not due to a lower mass flow rate in shorter CNTs, as discussed in [8]. On the contrary, the measured mass flow rate in short CNTs is comparable to that in longer CNTs. Therefore for a fixed pressure difference, the flow enhancement factor is directly proportional only to the CNT length.

3.2 Radial and Axial Profiles, Inlet and Outlet Effects

To investigate the radial structure of water transported in CNTs we measured the mean distribution of radial density for each CNT, see Fig. 6. We used 100 cylindrical bins of equal volume, centred radially inside the midpoint of the CNT, and covering a fixed length of 1 nm axially. The density within each bin is measured by summing the mass of water molecules contained over a specified period of time and dividing it by the axial sampling length and the number of averaging time-steps. Figure 6 shows that the average density profile is an-

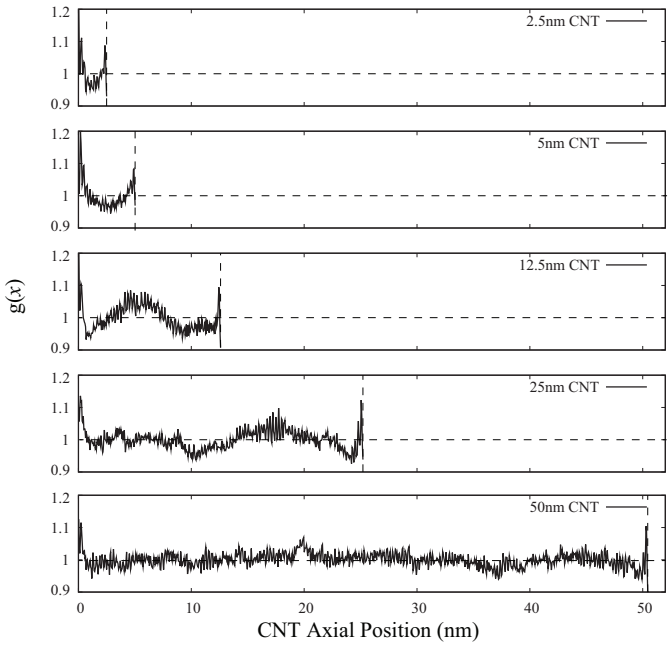

Fig. 7: Axial distribution functions for various CNT lengths.

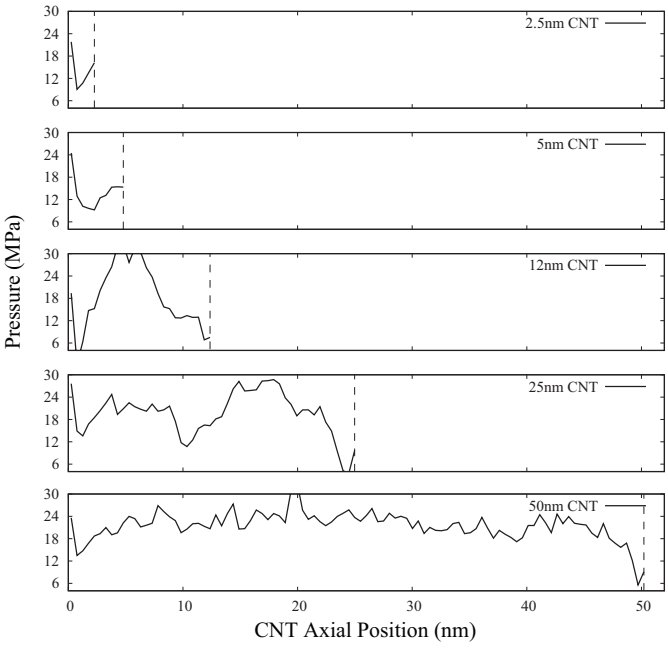

Fig. 9: Axial pressure profiles for various CNT lengths.

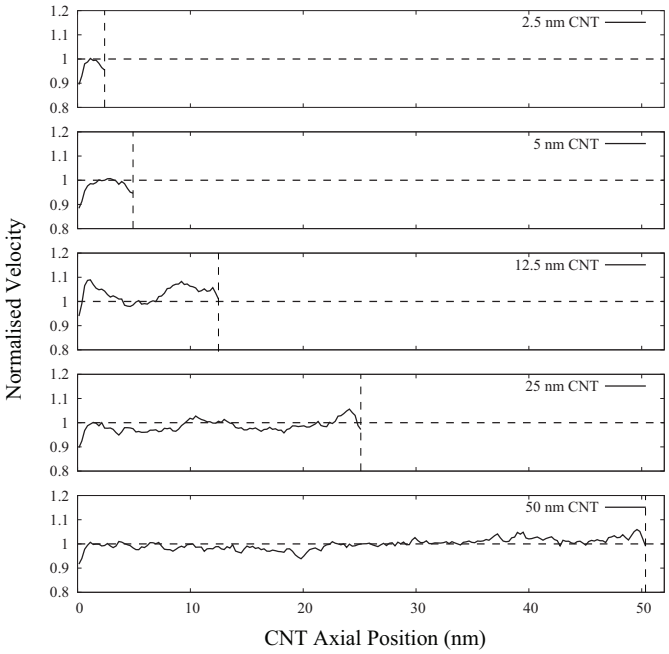

Fig. 8: Normalised axial velocity profiles for various CNT lengths.

nular, with a peak fluid density much higher than that of the reservoir (measured using the same technique). The total fluid density is dependent upon the definition of the occupied volume of the CNT, for which there is no consistency in the literature [24]. The distance between the peak density radius and the CNT surface corresponds to the interaction length of the Lennard-Jones potential between the carbon and oxygen atoms, σ_{CO}, and is unaffected by changes in CNT length. It is clear from Fig. 6 that even in very short channels molecular ordering is present, which may be a result of single or multiple-stranded molecular transport. Mattia and Gogotsi [12] imply that ordered diffusion takes a certain length to develop; if such a minimum length does exist, it must be very small. The minimal variation in the density peaks between the various CNTs can be explained by small changes in the axial profiles of density, shown in Fig 7. We note that our radial density profiles are similar to previous results [24] but the molecular arrangements may differ. The arrangement of water molecules inside CNTs is affected by a number of factors and the choice of water model is one of the most influential [25].

A significant insight into the transport behaviour of water through CNTs of varying length is available through examining the axial profiles of hydrodynamic properties. The axial distribution function (ADF) in each CNT is measured by using the binning technique described in [26] and presented in Fig 7, while velocity and pressure profiles are measured using standard techniques and shown in Figs. 8 and 9, respectively. In order to make comparison across the five CNTs, we use the same bin width for all axial profiles, and average over a time-period of 4 ns. We note that temperature profiles remain uniform across all the CNTs at ∼298 K. Pressure errors measured at the inlet/outlet of all the CNTs are within 15% of the reported values.

Water transport along a CNT is subject to inlet/outlet effects which manifest themselves in changes to fluid properties at the entrance and exit regions of the nanotube. The fluid has a higher density in these regions, with a corresponding drop in the fluid velocity. The peaks of the ADFs at the inlet and outlet of all CNTs may be caused by the simplified representation of the membrane, with the fluid inside the CNT interacting with the membrane walls. We note that this membrane model is commonly used in these types of simulations and that the inlet and outlet conditions are consistent for each CNT. The effect is to cause small dips in the axial density in the shorter CNTs and steady oscillations in the longer CNTs (diminishing in the 50 nm CNT). These slight changes in density do not affect the mass flow rate as the fluid velocity adjusts accordingly to conserve mass flow rate, as seen in Fig. 8.

3.3 Frictionless Flow?

The fact that the CNT length appears to have no influence on the mass flow rate is counter-intuitive from a hydrodynamic perspective (in fact, mass flow rate appears to slightly increase with length in some cases, as seen in Fig. 4). Consider the hydrodynamic expression for mass flow rate, Eq. 9: at such small scales, we might expect the viscosity to drop, and thus increase the mass flow rate – this is consistent with a hydrodynamic viewpoint. However, we would generally expect the viscosity to be independent of the length of the CNT, and so the question remains: why is mass flow rate constant for every L?

An explanation might be that the flow is effectively frictionless in the nanotube. But this cannot be the case, since a frictionless tube would imply an infinite flow rate for a fixed pressure drop, ΔP. The resolution to this paradox lies in Fig. 9. Clearly, the flow in the CNT, for each length, is not frictionless: the pressure at the inlet is greater than the pressure at the outlet in every case. This pressure loss, which results from frictional forces, appears mainly to result from a short development length at the inlet in the shorter CNTs, and a short exit region in the longer CNTs. So, in the longer CNT simulations, central "developed" regions are present that are effectively frictionless in contrast to the entrance/exit regions. As the CNT increases in length, these "frictionless" central regions cover proportionally more of the total CNT, to the point where extensions in CNT length result in roughly equal extensions to the central frictionless region. This may be why, beyond a certain CNT length (relative to the short entrance/exit region), the mass flow rate is relatively unaffected by changes in CNT length. However, the non-dependence on L appears to be evident at the smallest nanotube lengths considered here; more simulations at smaller nanotubes would be required to confirm this hypothesis.

Another reason why the flow in a CNT appears to behave as effectively frictionless is because the majority of viscous losses occur in the upstream reservoir, before the inlet (as evidenced by the order of magnitude difference between the inlet pressure and the upstream reservoir pressure, as seen in Fig. 9). It is possible that this pressure loss, which dwarfs the total head loss through the CNT, is independent of L since it occurs external to, and upstream of, the CNT. The question that remains unanswered is whether these large external pressure drops are physically realistic or merely an artefact of the MD domain setup for this type of CNT investigation. Either way, it is important to establish the source of these external losses and their role in determining CNT flow rate.

4 Conclusion

We have reported new results of non-equilibrium MD simulations of water transport through (7,7) CNTs, in particular how changing the CNT length affects the internal flow dynamics. Using new fluid pressure MD control techniques we have shown that under the same applied pressure difference an increase in CNT length has a negligible effect on the mass flow rate and fluid flow velocity. This results in larger flow enhancements over hydrodynamic expectations for longer CNTs. At a fixed pressure difference, the flow enhancement factor is directly proportional only to the CNT length.

By examining axial profiles of hydrodynamic properties we have demonstrated that entrance and exit effects are significant. Large viscous losses are experienced in these regions, and are shown by dips in the axial pressure profiles. In longer CNTs, central "developed" regions are present that are effectively frictionless. These regions extend proportionally with the length of the CNT, resulting in mass flow rates which are unaffected by an increase in CNT length.

Our simulation model is robust and can be adapted to a variety of applications, such as desalination, where the presence of periodic boundary conditions cannot accurately model the effect of concentration polarisation [10].

Acknowledgements The authors thank Rafael Delgado Buscalioni of the Universidad Autonoma de Madrid for useful discussions. This work is funded in the UK by the Engineering and Physical Sciences Research Council under grant EP/F002467/1, and by the Institution of Mechanical Engi-

neers. JMR would like to thank the Royal Academy of Engineering and the Leverhulme Trust for support through a Senior Research Fellowship. The authors are grateful for the comments of the reviewers on earlier drafts of this paper.

References

1. M. Majumder, N. Chopra, R. Andrew, B.J. Hinds, Nature **438**, 44 (2005)
2. J.K. Holt, H.G. Park, Y. Wang, M. Stadermann, A.B. Artyukhin, C.P. Grigoropoulos, A. Noy, O. Bakajin, Science **312**(5776), 1034 (2006)
3. M. Whitby, L. Cagnon, M. Thanou, N. Quirke, Nano Letters **8**(9), 2632 (2008)
4. J.A. Thomas, A.J.H. McGaughey, O. Kuter-Arnebeck, International Journal of Thermal Sciences **49**(2), 281 (2010)
5. B. Corry, Journal of Physical Chemistry B **112**(5), 1427 (2008)
6. S. Joseph, N.R. Aluru, Nano Letters **8**(2), 452 (2008)
7. M.E. Suk, A.V. Raghunathan, N.R. Aluru, Applied Physics Letters **92**(13), 133120 (2008)
8. J.A. Thomas, A.J.H. McGaughey, Physical Review Letters **102**(18), 184502 (2009)
9. B.J. Hinds, N. Chopra, T. Rantell, R. Andrews, V. Gavalas, L.G. Bachas, Science **303**(5654), 62 (2004)
10. B. Corry, Energy Environ. Sci. **4**, 751 (2011)
11. J.K. Holt, A. Noy, T. Huser, D. Eaglesham, O. Bakajin, Nano Letters **4**(11), 2245 (2004)
12. D. Mattia, Y. Gogotsi, Microfluidics and Nanofluidics **5**, 289 (2008)
13. A. Kalra, S. Garde, G. Hummer, Proceedings of the National Academy of Sciences of the United States of America **100**(18), 10175 (2003)
14. A. Striolo, Nano Letters **6**(4), 633 (2006). doi: 10.1021/nl052254u
15. G.B. Macpherson, N. Nordin, H.G. Weller, Communications in Numerical Methods in Engineering **25**(3), 263 (2009)
16. G.B. Macpherson, M.K. Borg, J.M. Reese, Molecular Simulation **33**(15), 1199 (2008)
17. G.B. Macpherson, J.M. Reese, Molecular Simulation **34**(1), 97 (2008)
18. M.K. Borg, G.B. Macpherson, J.M. Reese, Molecular Simulation **36**(10), 745 (2010)
19. OpenCFD Ltd. http://www.openfoam.com (2011)
20. T. Werder, J.H. Walther, R. Jaffe, T. Halicioglu, P. Koumoutsakos, Journal of Physical Chemistry B **107**(41), 1345 (2003)
21. E.G. Flekkøy, R. Delgado-Buscalioni, P.V. Coveney, Physical Review E **72**(2), 026703 (2005). doi: 10.1103/PhysRevE.72.026703
22. G.D. Fabritiis, R. Delgado-Buscalioni, P.V. Coveney, Journal of Chemical Physics **121**(24), 12139 (2004)
23. G. De Fabritiis, R. Delgado-Buscalioni, P.V. Coveney, Phys. Rev. Lett. **97**(13), 134501 (2006)
24. A. Alexiadis, S. Kassinos, Chemical Reviews **108**(12), 5014 (2008)
25. A. Alexiadis, S. Kassinos, Chemical Engineering Science **63**(10), 2793 (2008)
26. Y. Liu, Q. Wang, T. Wu, L. Zhang, The Journal of Chemical Physics **123**(23), 234701 (2005)